Electron spin noise under the conditions of nuclei-induced frequency focusing

Natalie Jäschke,[1] Frithjof B. Anders,[1] and Mikhail M. Glazov[2]
[1]*Lehrstuhl für Theoretische Physik II, Technische Universität Dortmund, Otto-Hahn-Straße 4, 44227 Dortmund, Germany*
[2]*Ioffe Institute, 194021 St.Petersburg, Russia*

(Received 24 May 2018; revised manuscript received 3 July 2018; published 24 July 2018)

We study theoretically the electron spin noise in quantum dots under nonequilibrium conditions caused by the pumping by a train of circularly polarized optical pulses. In such a situation, the nuclear spins are known to adjust in such a way that the electron spin precession frequencies become multiples of the pump pulse repetition frequency. This so-called phase synchronization effect was uncovered in A. Greilich *et al.* [Science **317**, 1896 (2007)] and termed nuclei-induced frequency focusing of electron spin coherence. Using the classical approach to the central spin model, we evaluate the nuclear spin distribution function and the electron spin noise spectrum. We show that the electron spin noise spectrum consists of sharp peaks corresponding to the phase synchronization conditions and directly reveal the distribution of the nuclear spins. We discuss the effects of nuclear spin relaxation after the pumping is over and analyze the corresponding evolution of nuclear spin distributions and electron spin noise spectra.

DOI: 10.1103/PhysRevB.98.045307

I. INTRODUCTION

During the last two decades, a new area of solid state physics, spintronics, was formed. It focuses on studying the effects of spin injection, detection, and nonmagnetic manipulation aiming at a deeper understanding the dynamics of charge carriers and nuclear spins with the long-term vision to provide a new generation of information processing devices. Particularly, the possibilities to use electron or nuclear spins as a building blocks for information processing are envisaged [1–4]. Both interesting fundamental physics and possible applications have made the effects of optical electron spin control in semiconductor quantum dots highly topical nowadays [5,6].

The primary focus lies in the nonmagnetic initialization, manipulation, and control of single spins [7–9]. Due to rather weak interaction of a single spin with light, the realization of such a single-spin device is rather challenging. In this regard, the control of the spin dynamics in quantum dot ensembles appears to be the much more favorable route [10,11]. However, the inevitable inhomogeneity in the quantum dot ensembles results in an efficient decoherence of the electron spins due to the nuclear fluctuations and the spread of the electron Landé factors.

It turns out that the role of the inhomogeneity can be effectively reduced by the nuclei-induced electron spin precession frequency focusing effect [12]. Under the excitation of the quantum dot ensemble by a periodic train of circularly polarized pulses with the repetition period T_R, the nuclear spins adjust in such a way that the electron spin precession frequency in each dot becomes a multiple of the repetition frequency π/T_R.

The origin of the focusing is the hyperfine coupling of electron and nuclear spins [10–13] accounted for by the central spin model (CSM) [14]. Several quantum-mechanical [15–17] or semiclassical [12,13,15,18–20] approaches have been proposed in order to describe this frequency focusing effect.

In the steady state of the periodically driven system, the Overhauser field distribution approaches a nonequilibrium function that significantly differs from its Gaussian shape in equilibrium [15–17,20]. This distribution function, which is crucial for testing the theoretical predictions and obtaining further control over the electron spin dynamics, is difficult to access directly in experiments.

Measurements of the electron spin dynamics [12,20] have been performed only on the periodically driven system where the pumping affects the nuclear spin states. Here, we suggest an alternative route to access the nuclear spin distribution by studying the electron spin fluctuations using the electron spin noise spectroscopy technique. Spin fluctuations can be measured by an off-resonant optical beam which does not significantly perturb the system [21–24] (see Refs. [25–27]) for reviews. We calculate the spectrum of the electron spin fluctuations under the conditions of the nuclei-induced frequency focusing effect. We demonstrate that the electron spin noise directly reveals the distribution of the nuclear spins. We show that by monitoring the electron spin fluctuations after the train of pump pulses has stopped the slow nuclear spin relaxation towards the equilibrium state can be accessed.

After a short introduction of the model in Sec. II, Sec. III demonstrates the relation between the electron spin dynamics and the shape of the Overhauser field distribution. We also present the evaluation of the electron spin noise and compare it with the Overhauser field distribution. The effect of the nuclear spin relaxation and its influence on the electron spin noise spectra are discussed on the last part of the Sec. III. A brief summary of the results is given in Sec. IV.

II. CENTRAL SPIN MODEL FOR NUCLEI-INDUCED ELECTRON SPIN PRECESSION FREQUENCY FOCUSING

In this section we formulate the semiclassical model of the electron and nuclear spin dynamics in a quantum dot under periodic optical excitation.

In a pump-probe experiment, a negatively charged semiconductor quantum dot is subjected to periodic laser pulses. We consider the Voigt geometry, i.e., the external magnetic field $\boldsymbol{B}_{\rm ext} \parallel x$ is orthogonal to the light propagation direction z which is also the growth axis of the quantum dot. The electron spin dephasing between two pulses is governed by the hyperfine interaction with the nuclear spin bath, which acts as an effective magnetic field. The circularly polarized pump pulse excites a X^- trion state consisting of two electrons in a spin singlet and a hole. Depending on the helicity of light, the resident electron becomes polarized (see Refs. [10,20,28–30] for details).

The classical equations of motion for the spin dynamics of the central spin model subject to an instantaneous laser pulse were derived in Ref. [20] (see also [18,30]) and are given by

$$\frac{d\boldsymbol{S}}{dt} = \left(\boldsymbol{b}_{\rm ext} + \sum_{k=1}^{N} a_k \boldsymbol{I}_k\right) \times \boldsymbol{S} + \gamma P_T \mathrm{e}^{-2\gamma t} \boldsymbol{e}_z, \tag{1a}$$

$$\frac{d\boldsymbol{I}_k}{dt} = (\zeta \boldsymbol{b}_{\rm ext} + a_k \boldsymbol{S}) \times \boldsymbol{I}_k. \tag{1b}$$

These equations are valid between two consecutive laser pulses for the time $t \in [0, T_{\rm R})$, where $T_{\rm R}$ is the pump pulse repetition period. The absorption of each pulse gives rise to an angular momentum transfer between photon and electron [28,29,31]. The full problem consisting of the photon absorption during pulse and emission during the trion decay can be simplified via the Lindblad formalism [16]. In the classical approach [11,20,29,32], the term $\gamma P_T e^{-2\gamma t}$ represents the increase of the electron spin vector in z direction due to the trion decay into the electron state. The quantity $P_{\rm T}$ is the efficiency of the trion photogeneration, and γ is the trion decay rate.

We treat the electron spin $\boldsymbol{S}$ and the spins of the nuclei $\boldsymbol{I}_k$ as classical vectors. The subscript k enumerates the N nuclei interacting with the electron spin. The applicability of the classical approach is justified in Refs. [20,33].

The coupled differential equations (1) are written in dimensionless units using the characteristic timescale T^* [34]

$$\frac{1}{(T^*)^2} = \sum_{k=1}^{N} A_k^2 \langle I_k^2 \rangle, \tag{2}$$

where we use $\langle I_k^2 \rangle = 1$ in the classical simulation. This timescale is determined by the fluctuations of the Overhauser field where A_k is the hyperfine coupling constant of the kth nuclear spin $\boldsymbol{I}_k$ to the central electronic spin $\boldsymbol{S}$. In Eqs. (1), the quantities $a_k = A_k T^*$ are the dimensionless coupling constants and the dimensionless magnetic field acting on the electron spin is $\boldsymbol{b}_{\rm ext} = g_{\rm e}\mu_{\rm B}\boldsymbol{B}_{\rm ext}T^*$, with μ_B being the Bohr magneton and $g_{\rm e}$ being the electron g factor. The parameter ζ denotes the ratio of the nuclear and electron magnetic moments. The electron spin dynamics within central spin model and its various extensions has been addressed within the semiclassical approach in a number of references [34–37].

Equation (1a) describes the electron spin precession in the total field comprising the external magnetic field and the field of the nuclei as well as the electron spin generation by the pump pulses: The efficiency of the trion photogeneration $P_{\rm T}$ is obtained from the electron spin z component before the pump pulse arrival $S_{{\rm bp},z}$ as

$$P_T = S_{{\rm bp},z} + \tfrac{1}{2}, \tag{3}$$

for the ideal π pulses considered in this paper. The electron spin after the pulse can by calculated via

$$\boldsymbol{S}_{\rm ap} = \tfrac{1}{2}\left(S_{{\rm bp},z} - \tfrac{1}{2}\right)\mathbf{e}_z. \tag{4}$$

The in-plane electron spin components are erased by the π pulse [29].

The dynamics of the nuclear spin $\boldsymbol{I}_k$ is influenced by the nuclear Zeeman effect and the Knight field $a_k \boldsymbol{S}$ [see Eq. (1b)]. The pump pulses do not produce any direct coupling to the nuclear spins so that the nuclear spin directions before and after the pump pulse arrival remain unchanged.

For a sufficiently long train of pump pulses, a steady-state situation is reached: the change of the nuclear spin vectors averaged over $T_{\rm R}$ vanishes and the electron spin dynamics becomes periodic. In this limit, the dimensionless Overhauser field in Eq. (1a),

$$\boldsymbol{b}_N = \sum_{k=1}^{N} a_k \boldsymbol{I}_k, \tag{5}$$

is replaced by a constant vector. The analysis of Eq. (1) in this frozen Overhauser field approximation demonstrates that the electron spin steady-state condition requires that one of two following conditions is satisfied [20]:

$$\omega = \omega_{{\rm e},n} \equiv \frac{2\pi n}{T_{\rm R}}, \tag{6a}$$

$$\omega = \omega_{{\rm o},n} \equiv \frac{1}{T_{\rm R}}\left[2\pi n + 2\arctan\left(\frac{\omega}{2\gamma}\right)\right], \; n \in \mathbb{Z} \tag{6b}$$

where ω is the electron spin precession frequency between the pulses,

$$\omega = |\boldsymbol{b}_{\rm ext} + \boldsymbol{b}_N|. \tag{7}$$

Note that even in the steady state the Overhauser field varies slightly due to the nuclear spin precession, particularly in a strong magnetic field. The rate, however, is much slower than ω justifying the frozen Overhauser field approximation.

The condition in Eq. (6a) depends only on the external magnetic field and the value of the pulse repetition rate $T_{\rm R}$, which corresponds to the so-called even resonances, i.e., even multiples of $\pi/T_{\rm R}$, while the condition in Eq. (6b) also includes the influence of the trion decay. For large external magnetic fields $b_{\rm ext}/\gamma \gg 1$, Eq. (6b) leads to resonance conditions with odd integer numbers $\omega_{{\rm o},n} T_{\rm R} = (2n+1)\pi$.

For the even resonance condition the central spin is fully aligned in the negative or positive z direction after the pulse, whereas the odd resonance conditions give a spin alignment of $\boldsymbol{S}_{\rm ap} = \mp\mathbf{e}_z/6$ depending on the helicity of light [16,18]. The detailed study of the electron and nuclear spin dynamics in the presence of periodic pumping is given in Ref. [20].

Starting from an unpolarized system where all spins are randomly oriented, the electron spin becomes polarized due to the pumping. The periodic pumping strongly amplifies the electron spin polarization in the quantum dots where the

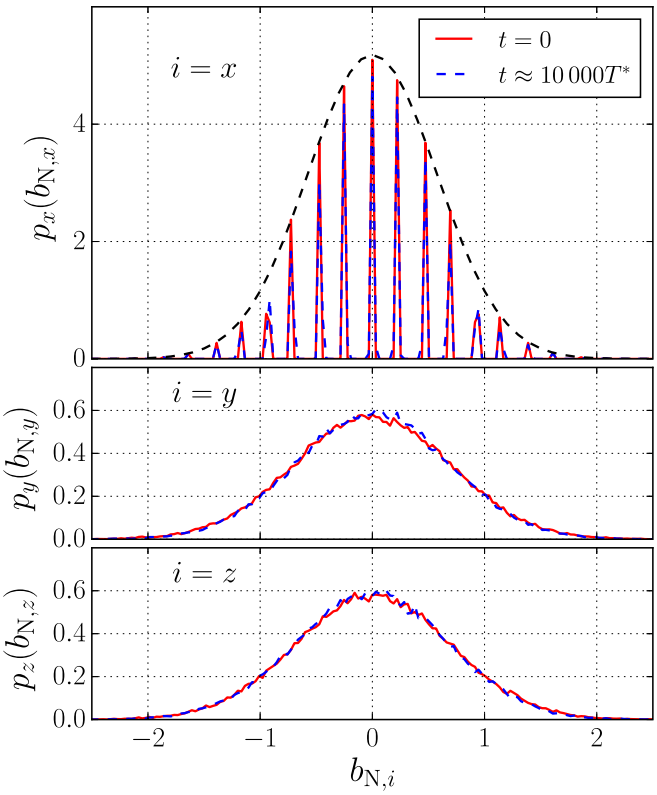

FIG. 1. Distributions of Cartesian components of the Overhauser field for the steady state of a periodically pulsed system. The initial distributions after the sequence of pump pulses has finished are shown in red. The Overhauser field distributions after approximately 10 000 T^* are shown in blue. The Gaussian envelopes are depicted in black.

conditions (6) are fulfilled. An electron spin revival can be observed [10,29,38]. Then, for a sufficiently long train of pump pulses, the hyperfine interaction leads to a rotation of nuclear spins and an eventual nuclear polarization in the direction of the external magnetic field in accordance with the resonance conditions (6) (see [20] for details). This is the nuclei-induced electron spin precession frequency focusing effect [10,12,18]. As a result, the distribution functions of the nuclear spins and, thus, the distribution of the Overhauser field is no longer Gaussian, but becomes peaked at certain particular values of $\boldsymbol{b}_{\mathrm{N}}$ where the conditions (6) hold. The Overhauser field distribution functions $p_i(b_{\mathrm{N},i})$, where $i = x$, y, or z is the Cartesian component after the pumping stage, are shown by red solid lines in Fig. 1.

III. SPIN DYNAMICS AND FLUCTUATIONS

In this section we present the results of calculations of the electron spin noise after the excitation by a train of pump pulses. We also demonstrate the relation between the electron spin fluctuations and the distribution of the Overhauser field.

The numerical simulations of the electron spin noise under the conditions of the nuclei-induced frequency focusing are carried out in the following way: We consider $N = 100$ nuclear spins and simulate $N_{\mathrm{C}} = 100\,000$ classical initial configurations for $\boldsymbol{I}_k(t = 0)$ such that the distribution functions of the Overhauser field components are given by

$$p_y(b_{\mathrm{N},i}) = p_z(b_{\mathrm{N},i}) = \mathcal{F}(b_{\mathrm{N},i}), \tag{8a}$$

$$p_x(b_{\mathrm{N},x}) = \sum_n \mathcal{F}(b_{\mathrm{N},x})[\delta(b_{\mathrm{N},x} - b_{\mathrm{e},n}) + \delta(b_{\mathrm{N},x} - b_{\mathrm{o},n})], \tag{8b}$$

where

$$\mathcal{F}(b_{\mathrm{N},i}) = \frac{1}{\sqrt{2\pi\sigma^2}} \exp\left(-\frac{b_{\mathrm{N},i}^2}{2\sigma^2}\right) \text{ for } i = x, y, z \tag{9}$$

is the Gaussian distribution with a variance $\sigma = 1/3$ providing the electron spin decoherence, $\delta(b)$ is the Dirac δ function, and $b_{\mathrm{e},n}$ ($b_{\mathrm{o},n}$) is the nuclear field which satisfies the condition Figs. (6a) [(6b)]. The shape of the Overhauser field distribution is a conjecture based on a scaling argument presented in Ref. [20].

We assume that the coupling constants are distributed according to

$$p_A(A) = -\frac{3}{2r_0^3}\frac{1}{A}\sqrt{\ln\left(\frac{A_{\max}}{A}\right)}, \tag{10}$$

with the dimensionless cutoff radius $r_0 = 1.5$ and $A_{\max} = 1$ [39]. A set $\{A_k\}$ is drawn from the distribution $p_A(A)$ and normalized via $a_k = A_k T^*$ using the definition (2). Further, we chose $T_{\mathrm{R}} = 13.5\,T^*$ for the repetition time of the pulses to make contact to the experiment and $\boldsymbol{b}_{\mathrm{ext}} = 2\pi K/T_{\mathrm{R}}\mathbf{e}_x$ with $K = 200$ for the external field corresponding to a physical value of approximately 2 T for typical quantum dot parameters. The relative strength of the nuclear Zeeman is given by $\zeta = 0.00125$, and the trion decay rate is set to $\gamma = 10/T^*$.

Our algorithm for the generation of a given Overhauser field distribution increases the precision with each additional nuclear spin (see Appendix). However, the restriction for the generation of the initial Overhauser field is an accepted deviation of

$$|\Delta b_{\mathrm{N},x}| = \left|\left(\sum_k a_k \boldsymbol{I}_{k,x}\right) - b_{\mathrm{o/e},n}\right| < 10^{-3}, \tag{11}$$

from the peak positions $b_{\mathrm{o/e},n}$ in each configuration which leads to a small but finite peak width instead of an ideal δ-function peak.

We investigated the evolution of the nuclear steady state in darkness, i.e., after stopping the pump pulses. At $t = 0$, the steady-state distribution defined in Eq. (8) is assumed, and the last pump pulse arrives. The peak width at this time is due to restrictions of the generation method, described in Eq. (11). This finite peak width mimics experiments in which a perfect frequency focusing cannot be achieved due to different nuclear spin relaxation mechanism or fluctuations in the pumping laser. In Fig. 1, we present the comparison between the initial steady-state Overhauser field distribution and its evolution after $t = 1000T_{\mathrm{R}} \approx 10\,000T^*$. Only marginal changes are observable, and the peak structure is essentially preserved on this timescale.

This phenomenon will be analyzed more deeply in the following sections, with the additional focus on the electron spin dynamics.

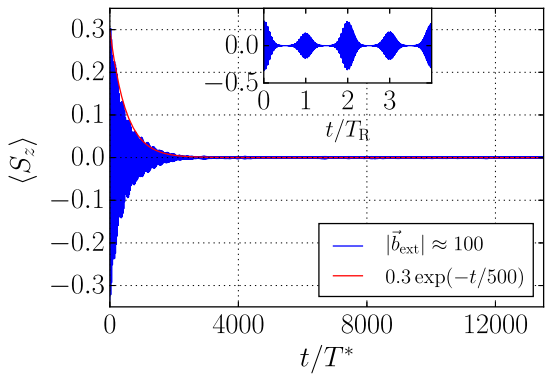

FIG. 2. Central spin dynamics starting from the steady state of a pulsed system. The red line gives the envelope of the electron spin revival decay. The inset shows spin dynamics on the shorter timescale.

A. Electron spin dynamics after the pumping

Figure 2 shows the electron spin dynamics $\langle S_z(t)\rangle$ after the last pump pulse using the Overhauser field distribution introduced in the previous section. The electron spin precession in the total magnetic field $\boldsymbol{b}_{\rm ext} + \boldsymbol{b}_{\rm N}$ is very fast so that field-induced spin beats are not resolvable in the figure. On a long timescale, the electron spin envelope function decays with time due to a finite width of peaks in $p_x(b_{{\rm N},x})$, while the generated Overhauser field peak has a rectangular shape for $N = 100$. The "edges" of this distribution decay fast due to nuclear spin precession and generate a nearly Lorentzian-shaped peak. Indeed, if the Overhauser field peaks are approximated by a Lorentzian function, the long-time decay of the electron spin polarization envelope is described by the exponential law $\langle S_z(t)\rangle \sim \exp(-t/T_{\rm D})$ with $T_{\rm D}$ being the decay time inversely proportional to the Lorentzian width. The shape of the envelope of the electron spin decay was derived via Fourier transformation of a single peak shape. We added an exponential function with $T_{\rm D} = 500T^*$ (red solid line) as a guide to the eye into Fig. 2, demonstrating a reasonable agreement with the envelope function of our simulation. Naturally, different peak shapes provide different time envelopes of electron spin beats. In our simulations, the value of $T_{\rm D} \sim 10^3 T^*$ is limited by the accuracy of the randomly generated Overhauser field distribution (11).

On a timescale of a few $T_{\rm R}$, the revivals of the electron spin polarization are depicted in the inset to Fig. 2 resolving the electron spin dynamics on a much shorter timescale up to $t = 4T_{\rm R}$. These revivals at integer multiples of $T_{\rm R}$ are a clear signature of the nuclei-induced spin precession frequency focusing: The most probable spin precession frequencies are, in agreement with Eqs. (6), the multiples of $\pi/T_{\rm R}$. The alternating revival strengths shown in the inset result from the interplay of the even and odd resonance frequencies. For the larger revival amplitudes, the spin configurations with even and odd resonance frequencies align: $\boldsymbol{S}_{\rm even} = \mp\mathbf{e}_z/2$ and $\boldsymbol{S}_{\rm odd} = \mp\mathbf{e}_z/6$ (for σ^+/σ^- pumping), whereas for every second $T_{\rm R}$ distance the contributions due to even and odd resonances point in the opposite directions: $\boldsymbol{S}_{\rm even} = \mp\mathbf{e}_z/2$ and $\boldsymbol{S}_{\rm odd} = \pm\mathbf{e}_z/6$.

While the central spin shows a clearly recognizable relaxation, the Overhauser field distribution is almost conserved as discussed in the previous section. This implies that the electron spin will interact with an already prepared nuclear spin system once the pulse sequence is switched on again. Therefore, it can be seen as an indicator for the reemerging instant revival after several minutes in darkness as it was observed in experiments reported in Ref. [12].

B. Electron spin noise

The spin noise is characterized by the second-order spin correlator $\langle S_z(t+t')S_z(t')\rangle$ in the time domain. In the frequency domain, the electron spin noise spectrum is obtain by its Fourier transformation:

$$\left(S_z^2\right)_\omega(t') = \int_{-\infty}^{\infty} e^{-i\omega t}\langle S_z(t+t')S_z(t')\rangle dt\,. \tag{12}$$

We stress that the spin noise spectrum is dependent on the absolute time t' due to the nonequilibrium and nonstationary situation: at $t' = 0$ the nuclear spin system is described by the distribution functions (8), which is strongly different from the equilibrium Gaussian, and where an average electron spin polarization is found (see Fig. 2).

However, electron and nuclear spin dynamics are characterized by timescales which differ by several orders of magnitude. The electron spin dephasing takes place on a timescale of $T_{\rm D}$ related with incomplete focusing (see Sec. III A). In contrast, the nuclear spin relaxation characterized by the time constant $T_{1,{\rm N}}$ is extremely slow and can last for tens of minutes. Hereafter, we assume that

$$T_{1,{\rm N}} \gg t' \gg T_{\rm D}, \tag{13}$$

which allows us to consider the system in quasisteady state: the spin correlation function $\langle S_z(t+t')S_z(t')\rangle$ and the spin noise spectrum $(S_z^2)_\omega$ becomes independent on the time t'. In agreement with the general theory of nonequilibrium spin fluctuations [40,41], the correlation functions of the fluctuations obey the same set of equations as the average values. Thus, Eq. (1a) (with $P_{\rm T} = 0$) can be considered as the equation for the electron spin correlators $\langle S_\alpha(t+t')S_z(t')\rangle$ as functions of time t. Also, it has to be taken into account that the nuclear spin dynamics in Eq. (1b) is driven by the electron spin fluctuations. The initial nuclear spin distribution is given by (8), while the equal time electron correlation functions are given by $\langle S_z(t)S_z(t)\rangle = \frac{1}{4}$, and the cross correlators vanish: $\langle S_y(t)S_z(t)\rangle = \langle S_x(t)S_z(t)\rangle = 0$, which follows from the quantum-mechanical definition of the electron spin. Note that due to condition (13) the initial correlation of the electron spin orientation and Overhauser field can be disregarded. The electron spin correlators and spin noise spectra can weakly depend on t' due to the nuclear spin dynamics.

In order to fulfill the requirement $T_{\rm D} \ll t'$, we used as initial condition the Overhauser field distribution obtained by a full simulation of the equations of motion for $t' = 1000T_{\rm R} \approx 10\,000T^*$ after the pump pulses have stopped (see Fig. 1).

Figure 3(a) shows the spin noise spectrum $(S_z^2)_\omega(t')$ calculated by the full numerical solution of the set of Eqs. (1) and the nonequilibrium Overhauser field distribution. The spin noise spectrum consists of a series of peaks at the electron spin precession frequencies ω satisfying the resonance conditions (6). The calculations demonstrate that the electron

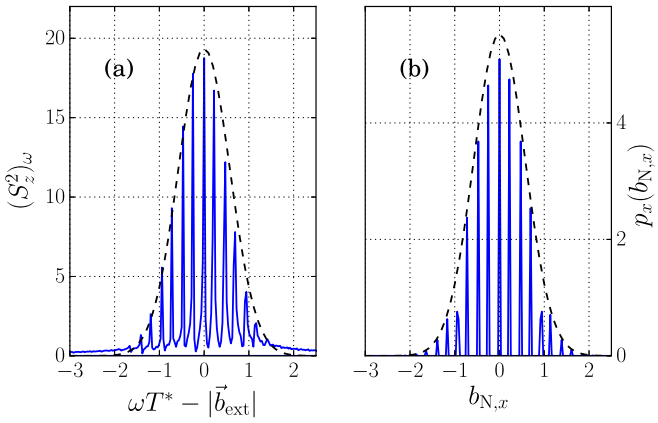

FIG. 3. (a) Spin noise spectrum of the full numerical simulation. (b) The initial Overhauser field distribution taken from Fig. 1 at $t' = 1000T_{\rm R} \approx 10\,000T^*$.

spin correlation function and, correspondingly, the spin noise spectrum is almost independent of t', implying a very slow nuclear spin relaxation.

The fact that the nuclear fields are almost static allows for the evaluation of the spin noise spectrum semiclassically: the model developed in Ref. [42] assumes that the nuclear fields are frozen. A similar model has been employed in Refs. [43,44] to address the electron spin fluctuations in the presence of dynamical nuclear polarization. In this model, the electron spin noise spectrum directly reflects the distribution of the effective magnetic field acting on the electron spin. It is given, up to a common factor, by

$$\left(S_z^2\right)_\omega(t') \propto p_x(\omega - b_{{\rm ext},x}). \tag{14}$$

In order to show the connection between the full numerical simulation and the analytical prediction, the corresponding initial distribution of the nuclear fields is added as Fig. 3(b) being in a good agreement with the full calculation presented in Fig. 3(a). Slight discrepancies are related to neglecting the nuclear spin dynamics in Eq. (14) and to the contributions to the electron spin precession frequency of the nuclear field components transversal to the external magnetic field. This analysis confirms that the information about the nuclear spin polarization can be accessed by the spin noise spectrum $(S_z^2)_\omega(t')$. The electron spin fluctuations can be measured via the detection of fluctuations of the polarization plane of the light beam transmitted through or reflected from the sample. Indeed, a fluctuation of spin polarization (i.e., magnetization) gives rise to a stochastic Faraday rotation of the polarization plane of light, which can be readily detected in optical experiments. This nonperturbative way to measure the electron spin noise optically was first suggested and realized by Alexandrov and Zapasskii [21] and later adapted by various experimental groups [23,24,45] (see Refs. [25,26] for review).

C. Inclusion of a phenomenological relaxation of the Overhauser field

As we have seen in Fig. 1 the Overhauser field distribution is almost conserved for long times after the pulse sequence. The distribution of the coupling constants a_k can induce some decay

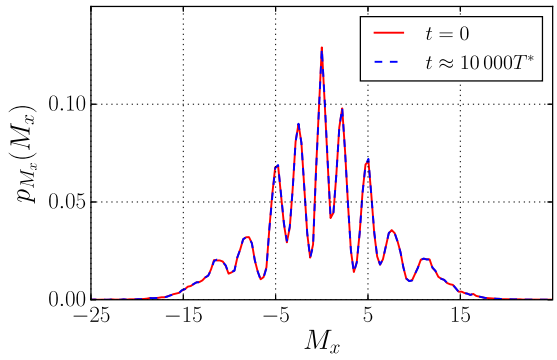

FIG. 4. The distribution of the total nuclear spin in x direction M_x corresponding to the Overhauser field shown in Fig. 1 is conserved.

of the Overhauser field similarly to the processes described in Refs. [33,34,46,47], however, this decay is quite minor. This can be ascribed to the fact that the component of the total spin

$$\boldsymbol{F} = \boldsymbol{S} + \sum_k \boldsymbol{I}_k \tag{15}$$

of the interacting electron-nuclear system parallel to the external field is conserved. Since the nuclear spin bath size is large, the total nuclear spin $\boldsymbol{M} = \sum_k \boldsymbol{I}_k \propto \sqrt{N}$ constitutes the dominating contribution to $\boldsymbol{F}$:

$$\langle F_x \rangle \approx \langle M_x \rangle = \text{const}. \tag{16}$$

Hence, a variation of the electron spin x component can be neglected in comparison to the constant contribution $\langle M_x \rangle \propto \sqrt{N}$. It is noteworthy to distinguish the approximatively conserved total nuclear spin polarization $\langle M_x \rangle$ in an external field applied in x direction from the slowly varying Overhauser field for a finite spread of the coupling constants a_k. Only in the case of the box model with $a_k = a\ \forall\ k$ the difference between Overhauser field and total nuclear spin reduces to the constant a and, therefore, the Overhauser field distribution is also static. To illustrate the difference, we present the the total nuclear spin distribution in x direction, $p_{M_x}(M_x)$, in Fig. 4 for the system parameters used in Fig. 1. While a close inspection of Figs. 1 and 3(b) reveals the slow time evolution of $p_x(b_{N,x})$, $p_{M_x}(M_x)$ remains constant for the simulation times $t < 10\,000T^*$.

In a real system, however, several different processes such as the dipole-dipole interaction between the nuclear spins [48], fluctuating quadrupolar splittings of nuclei [49], due to the recharging processes and the photoexcitation [12,50] contribute to the nuclear spin relaxation that occurs on a much larger timescale as considered up to now. In order to analyze this effect, we employ the phenomenological approach where we (i) use the box model for simplicity, (ii) calculate the electron spin noise spectrum via the semiclassical equation (14), and (iii) introduce the nuclear spin relaxation by means of a kinetic equation for the distribution function p_{M_x}.

The longitudinal nuclear spin relaxation time $T_{1,\rm N}$ is much larger than any timescale related to the electron spin dynamics. As a result, we can regard the Overhauser field as static in a time interval while we investigate the electron spin dynamics of the correlation function $\langle S_z(t'+t)S_z(t')\rangle$. As we can gather from Fig. 2 the electron spin has vanished after a relatively short amount of time. Therefore, we will assume an unpolarized

central spin at the beginning of each time interval starting at t' with a static Overhauser field distribution at the time t'.

To achieve a decay of the distribution of the total nuclear spin component M_x, spin flips decreasing or increasing M_x have to be taken into account. The general time evolution of the distribution function $p_{M_x}(M_x;t')$ is given by the following rate equation:

$$\frac{dp_{M_x}(M_x;t')}{dt'} = W_\downarrow(M_x+1)p_{M_x}(M_x+1;t') + W_\uparrow(M_x-1)p_{M_x}(M_x-1;t') - [W_\downarrow(M_x)+W_\uparrow(M_x)]p_{M_x}(M_x;t'). \quad (17)$$

$W_{\uparrow/\downarrow}$ are the nuclear spin-flip probabilities, where $\uparrow$ denotes the process of increasing M_x by 1 and $\downarrow$ denotes the process of decreasing M_x by 1. Note that dipole-dipole interaction between the nuclei and the quadrupole splittings can result in the change of M_x by 2, however, the inclusion of such additional processes does not qualitatively affect the results.

Now, we employ the box model: $p_x(b_{\mathrm{N},x})$ and $p_{M_x}(M_x)$ differ only by a constant prefactor. At $t'=0$, the time at the end of the pumping, the analytic Overhauser field distribution stated in Eq. (8) is used, and the distribution function $p_{M_x}(M_x;t')$ is normalized according to

$$\sum_{M_x} p_{M_x}(M_x;t') = 1$$

at any time. Reminding that $1 \ll |M_x| \ll N$ holds in real systems, we can convert the discrete rate equation (17) into a partial differential equation

$$\frac{\partial p_{M_x}(M_x;t')}{\partial t'} = \frac{1}{T_{1,\mathrm{N}}}\frac{\partial}{\partial M_x}\left[M_x p_{M_x}(M_x;t') + \frac{M^2}{3}\frac{\partial}{\partial M_x}p_{M_x}(M_x;t')\right], \quad (18)$$

in the continuum limit which is an analog of the Fokker-Planck equation in kinetic theory [40]. We made use of the expressions

$$W_\uparrow(M_x) = W_1(N/2 - M_x), \quad (19)$$

$$W_\downarrow(M_x) = W_1(N/2 + M_x), \quad (20)$$

with W_1 being the probability of a single spin flip, and the factors $N/2 \pm M_x$ describing the number of choices for a nuclear spin to flip, which are valid in the high-temperature approximation [48]. In Eq. (18), $T_{1,\mathrm{N}}$ denotes the longitudinal relaxation time of the nuclear spin governing the exponential decay of the average nuclear spin $\overline{M}_x(t') = \int dM_x M_x p_{M_x}(M_x;t')$:

$$\frac{\partial \overline{M}_x}{\partial t'} = -\frac{\overline{M}_x(t')}{T_{1N}}, \quad (21)$$

and $M^2 = |I^2|N$ is the square of the total spin of the nuclei. The steady-state solution of Eq. (18) corresponds to the unpolarized bath with the Gaussian distribution function of the nuclear spins,

$$p_{M_x}(M_x) = \frac{1}{2}\sqrt{\frac{6}{\pi M^2}}\exp\left(-\frac{3M_x^2}{2M^2}\right), \quad (22)$$

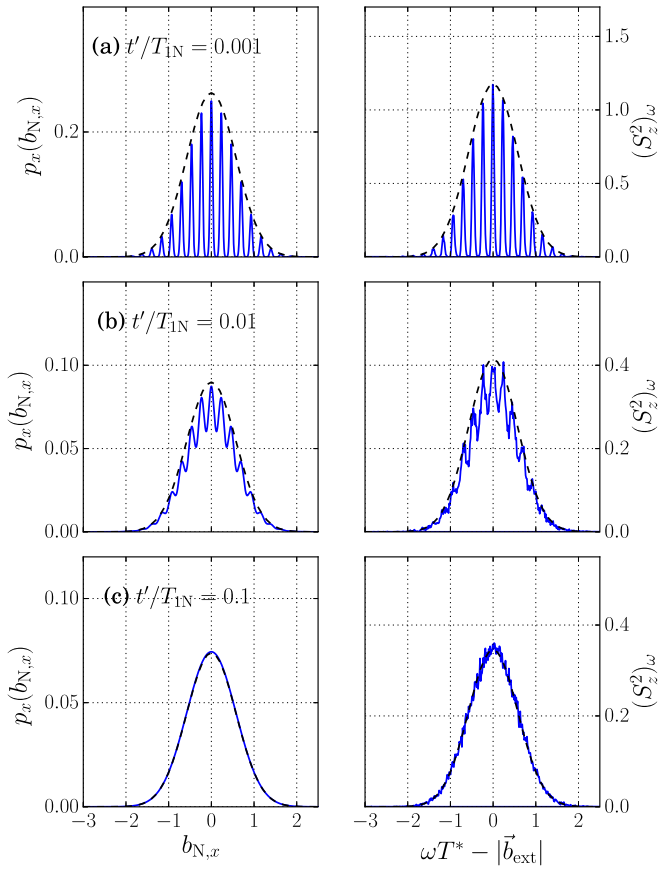

FIG. 5. Left side: normalized Overhauser field distribution. Right side: normalized spin noise spectra for (a) $t'/T_{1,\mathrm{N}} = 0.001$, (b) 0.01, and (c) 0.1. The spin noise spectra are shifted by the frequency of the external magnetic field for better comparability.

with the variance

$$\int p_{M_x}(M_x)M_x^2 dM_x = M^2/3. \quad (23)$$

For the investigation of the time dependency of the Overhauser field distribution, we use Eq. (8) as the initial condition. The broadening is determined by the variance $\sigma_\mathrm{P}^2 = 10^{-4}$ introduced when replacing the δ functions in Eq. (8) by the Gaussian as

$$\delta(x) \to \frac{1}{\sqrt{2\pi\sigma_\mathrm{P}^2}}\exp\left(-\frac{x^2}{2\sigma_\mathrm{P}^2}\right).$$

As $\lim_{\omega\to\infty}\arctan[\omega/(2\gamma)] = \pi/2$ in Eq. (6b) holds for large external magnetic fields of several Tesla used in the experiments [12], we set the second set of peaks exactly at odd multiples of π/T_R.

The differential equation (18) can be analytically solved by a Fourier transformation and by using a separation of variables. Note that the solution of Eq. (18) depends only on the ratio $t'/T_{1,\mathrm{N}}$. The shape of the Overhauser field distribution is calculated for the times $t'/T_{1,\mathrm{N}} = 10^{-3}$, 10^{-2}, and 10^{-1} and shown in Fig. 5, left column.

The Overhauser fields are randomly generated from these distributions for each classical configuration. For these different times, the autocorrelation functions of the central spin

$\langle S_z(t'+t)S_z(t')\rangle$ are calculated by full numerical simulations of (1) and their Fourier transformations give the corresponding electron spin noise spectra. The results are shown in the right column of Fig. 5.

The x component of the Overhauser field distribution shows a clear decay of the peaked substructure inside its Gaussian envelope driven by the nuclear spin relaxation processes parametrized by $T_{1,\mathrm{N}}$. The electron spin noise spectrum traces remarkably the time evolution of the Overhauser field distribution and, therefore, gives direct access to the time constant of the nuclear spin relaxation. Both distributions match very well apart from normalization and the shift of the spin noise spectra by the Larmor precession frequency which is given by the external magnetic field $|\boldsymbol{b}_{\mathrm{ext}}|$. For longer times, the nuclear spin bath relaxes to the Gaussian equilibrium state (9). Thus, by monitoring the spin noise as a function of time t' after the preparation of the nuclear spin system, one can obtain the time evolution of the nuclear spin system and extract the parameter $T_{1,\mathrm{N}}$, the nuclear spin-lattice relaxation time.

Noteworthy, a similar protocol of electron spin noise measurements can be applied in the course of the focusing process, i.e., starting from the unpolarized nuclear state and interrupting the pulse train to measure the electron spin noise. In such a case, the formation of the peaked distribution of nuclear states can be monitored and the focusing time can be estimated and compared with model predictions [12,16–20].

IV. CONCLUSION

In this work we demonstrate that the distribution of the nuclear spins can be readily determined from the electron spin noise spectrum under the conditions of the nuclei-induced electron spin precession frequency focusing effect.

Based on simulations of the nuclei-spin dynamics under the effect of a pump pulse train [20], a steady-state distribution of Overhauser fields acting on the electron is extrapolated. The distribution of the longitudinal, i.e., parallel to an external magnetic field, component of the Overhauser field features sharp peaks at the resonant conditions (6). The numerical simulations in Ref. [20] indicate that while the evolution from a Gaussian to the steady-state Overhauser field distribution of the pulsed system is dependent on the distribution of hyperfine interaction coupling constants, the steady-state function within the CS does not depend on this distribution. The final distribution function is given by a set of δ peaks at the resonance conditions whose widths are determined by the numerical error in the simulation. In real systems, additional interactions such as the nuclear electric quadrupolar interaction as well as the nuclear dipole-dipole interactions will modify the peak shape. The electron spin precession frequency in the total field (being sum of external and Overhauser field), is commensurable with the pump pulse repetition frequency.

In the numerical simulation, we used two different representations of the δ peak located at the resonance conditions: a box-shaped peak distribution with a very small width of 10^{-3} in dimensionless units and a very narrow Gaussian peak for the evolution of the Fokker-Planck equations.

For the simulation of the equations of motion introduced in Sec. II, we employed the rectangular-shaped peaks as representation of the steady-state δ peaks of the Overhauser field distribution. As a result the dynamics described by Eqs. (1) the rectangular peaks get slightly broadened and acquire a Lorentzian shape with a comparable width after a long simulation time of $5000T^*$, illustrating the very slow change of the distribution function with time. The electronic-nuclear spin correlations that were induced by the laser pumping are suppressed by the dephasing after that time.

It was shown that the Overhauser field distribution is stable for a macroscopically long time after the end of pulsing due to the angular momentum component conservation in the electron-nuclear spin system. The calculated electron spin noise spectrum closely follows the Overhauser distribution function.

Since the numerical simulations are very costly, we resort to a kinetic equation for the slow nuclear spin relaxation in order to access the long-time limit. These equations can be easily solved using a Gaussian representation of the initial narrow steady-state δ peaks of the Overhauser field distribution. The evolution of the electron spin noise spectrum is driven by this slow nuclear spin relaxation, which is accounted for by a simple kinetic equation. We demonstrate that the nuclear relaxation toward the structureless Gaussian distribution is also directly revealed in the electron spin fluctuations. The phenomenologically introduced nuclear spin relaxation time $T_{1,\mathrm{N}}$ can be determined experimentally by tracking the spin noise spectrum as function of time.

ACKNOWLEDGMENTS

We are grateful to A. Fischer, I. Kleinjohann, and P. Schering for discussions. We acknowledge the financial support by the Deutsche Forschungsgemeinschaft and the Russian Foundation of Basic Research through the transregio TRR 160. M.M.G. is grateful to Russian foundation for basic research Projects No. 17-02-00383 and No. 15-52-12012 and Russian President Grant No. MD-1555.2017.2 for partial support. The authors gratefully acknowledge the computing time granted by the John von Neumann Institute for Computing (NIC) under Project No. HDO09 and provided on the supercomputer JUQUEEN at the Jülich Supercomputing Centre.

APPENDIX: GENERATION OF THE NUCLEAR SPIN BATH

The classical configurations are assigned to the peaks depending on the weight of the peak. The algorithm for each Overhauser field peak $b_{\mathrm{N},i}$ is then as follows:

(1) I_1 is randomly generated on the unit sphere. $b_{\mathrm{N},1} = a_1 I_1$;

(2) subsequent $a_k I_k$ with I_k randomly generated are added if $b_{\mathrm{N},k-1} - b_{\mathrm{N},i} > b_{\mathrm{N},k} - b_{\mathrm{N},i}$ with $b_{\mathrm{N},k} = \sum_{j=1}^{k} a_j I_j$.

The computation time in the algorithm grows the smaller the peak width gets. Therefore, a cutoff has to be set [Eq. (11)]. This $|\Delta b_{N,x}|$ determines the peak width and still leads to acceptable computation times for the generation of the distribution. Then, if the number of nuclear spins is great enough to reach the precision of $|\Delta b_{N,x}|$ before all nuclear spins are generated the peak is a unitary transformation inside the boundaries $\pm|\Delta b_{N,x}|$. However, a note is in order: since the number of configurations per peak vary, so does the noise.

For the lesser weighted peaks, the influence of the noise to the distribution in the peak can be substantial. Therefore, an analytical representation of the Overhauser field distribution is hard to obtain.

[1] C. H. Bennett and D. P. DiVincenzo, Nature (London) **404**, 247 (2000).
[2] L. K. Grover, Phys. Rev. Lett. **79**, 325 (1997).
[3] D. Loss and D. P. DiVincenzo, Phys. Rev. A **57**, 120 (1998).
[4] R. Hanson, L. P. Kouwenhoven, J. R. Petta, S. Tarucha, and L. M. K. Vandersypen, Rev. Mod. Phys. **79**, 1217 (2007).
[5] *Spin Physics in Semiconductors*, 2nd ed., Springer Series in Solid-State Sciences 157, edited by M. I. Dyakonov (Springer, Berlin, 2017).
[6] O. Gywat, H. Krenner, and J. Berezovsky, *Spins in Optically Active Quantum Dots: Concepts and Methods* (Wiley, Hoboken, NJ, 2010).
[7] M. H. Mikkelsen, J. Berezovsky, N. G. Stoltz, L. A. Coldren, and D. D. Awschalom, Nat. Phys. **3**, 770 (2007).
[8] D. Press, K. De Greve, P. L. McMahon, T. D. Ladd, B. Friess, C. Schneider, M. Kamp, S. Hofling, A. Forchel, and Y. Yamamoto, Nat. Photonics **4**, 367 (2010).
[9] C. Arnold, J. Demory, V. Loo, A. Lemaître, I. Sagnes, M. Glazov, O. Krebs, P. Voisin, P. Senellart, and L. Lanco, Nat. Commun. **6**, 6236 (2015).
[10] D. R. Yakovlev and M. Bayer, in *Spin Physics in Semiconductors*, 2nd ed., edited by M. I. Dyakonov (Springer, Berlin, 2017), p. 155.
[11] M. M. Glazov, Phys. Solid State **54**, 1 (2012).
[12] A. Greilich, A. Shabaev, D. R. Yakovlev, A. L. Efros, I. A. Yugova, D. Reuter, A. D. Wieck, and M. Bayer, Science **317**, 1896 (2007).
[13] S. G. Carter, A. Shabaev, S. E. Economou, T. A. Kennedy, A. S. Bracker, and T. L. Reinecke, Phys. Rev. Lett. **102**, 167403 (2009).
[14] M. Gaudin, J. Phys. **37**, 1087 (1976).
[15] M. Petrov and S. Yakovlev, J. Exp. Theor. Phys. **115**, 326 (2012).
[16] W. Beugeling, G. S. Uhrig, and F. B. Anders, Phys. Rev. B **94**, 245308 (2016).
[17] W. Beugeling, G. S. Uhrig, and F. B. Anders, Phys. Rev. B **96**, 115303 (2017).
[18] M. M. Glazov, I. A. Yugova, and A. L. Efros, Phys. Rev. B **85**, 041303 (2012).
[19] V. L. Korenev, Phys. Rev. B **83**, 235429 (2011).
[20] N. Jäschke, A. Fischer, E. Evers, V. V. Belykh, A. Greilich, M. Bayer, and F. B. Anders, Phys. Rev. B **96**, 205419 (2017).
[21] E. Aleksandrov and V. Zapasskii, Zh. Eksp. Teor. Fiz. **81**, 132 (1981) [JETP **54**, 64 (1981)].
[22] J. L. Sørensen, J. Hald, and E. S. Polzik, Phys. Rev. Lett. **80**, 3487 (1998).
[23] S. A. Crooker, D. G. Rickel, A. V. Balatsky, and D. L. Smith, Nature (London) **431**, 49 (2004).
[24] M. Oestreich, M. Römer, R. J. Haug, and D. Hägele, Phys. Rev. Lett. **95**, 216603 (2005).
[25] V. S. Zapasskii, Adv. Opt. Photon. **5**, 131 (2013).
[26] J. Hübner, F. Berski, R. Dahbashi, and M. Oestreich, Phys. Status Solidi B **251**, 1824 (2014).
[27] N. A. Sinitsyn and Y. V. Pershin, Rep. Prog. Phys. **79**, 106501 (2016).
[28] A. Greilich, R. Oulton, E. A. Zhukov, I. A. Yugova, D. R. Yakovlev, M. Bayer, A. Shabaev, A. L. Efros, I. A. Merkulov, V. Stavarache, D. Reuter, and A. Wieck, Phys. Rev. Lett. **96**, 227401 (2006).
[29] I. A. Yugova, M. M. Glazov, E. L. Ivchenko, and A. L. Efros, Phys. Rev. B **80**, 104436 (2009).
[30] M. M. Glazov, J. Appl. Phys. **113**, 136503 (2013).
[31] E. Barnes and S. E. Economou, Phys. Rev. Lett. **107**, 047601 (2011).
[32] E. A. Zhukov, D. R. Yakovlev, M. Bayer, M. M. Glazov, E. L. Ivchenko, G. Karczewski, T. Wojtowicz, and J. Kossut, Phys. Rev. B **76**, 205310 (2007).
[33] G. Chen, D. L. Bergman, and L. Balents, Phys. Rev. B **76**, 045312 (2007).
[34] I. A. Merkulov, A. L. Efros, and M. Rosen, Phys. Rev. B **65**, 205309 (2002).
[35] R. Kubo and T. Toyabe, in *Magnetic and Electric Resonance and Relaxation*, edited by R. Blinc (North-Holland, Amsterdam, 1967), p. 810.
[36] K. Schulten and P. G. Wolynes, J. Chem. Phys. **68**, 3292 (1978).
[37] A. Khaetskii, D. Loss, and L. Glazman, Phys. Rev. B **67**, 195329 (2003).
[38] A. Greilich, D. R. Yakovlev, A. Shabaev, A. L. Efros, I. A. Yugova, R. Oulton, V. Stavarache, D. Reuter, A. Wieck, and M. Bayer, Science **313**, 341 (2006).
[39] J. Hackmann and F. B. Anders, Phys. Rev. B **89**, 045317 (2014).
[40] L. Landau and E. Lifshitz, *Physical Kinetics* (Butterworth-Heinemann, Oxford, 1981).
[41] S. Gantsevich, V. Gurevich, and R. Katilius, La Riv. Nuovo Cimento **2**, 1 (1979).
[42] M. M. Glazov and E. L. Ivchenko, Phys. Rev. B **86**, 115308 (2012).
[43] D. S. Smirnov, Phys. Rev. B **91**, 205301 (2015).
[44] I. I. Ryzhov, G. G. Kozlov, D. S. Smirnov, M. M. Glazov, Y. P. Efimov, S. A. Eliseev, V. A. Lovtcius, V. V. Petrov, K. V. Kavokin, A. V. Kavokin, and V. S. Zapasskii, Sci. Rep. **6**, 21062 (2016).
[45] S. A. Crooker, L. Cheng, and D. L. Smith, Phys. Rev. B **79**, 035208 (2009).
[46] S. I. Erlingsson and Y. V. Nazarov, Phys. Rev. B **70**, 205327 (2004).
[47] W. A. Coish and D. Loss, Phys. Rev. B **70**, 195340 (2004).
[48] A. Abragam, *Principles of Nuclear Magnetism*, Oxford Science Publications (Oxford University Press, Oxford, 2002).
[49] D. Paget, T. Amand, and J.-P. Korb, Phys. Rev. B **77**, 245201 (2008).
[50] D. S. Smirnov, P. Glasenapp, M. Bergen, M. M. Glazov, D. Reuter, A. D. Wieck, M. Bayer, and A. Greilich, Phys. Rev. B **95**, 241408 (2017).